Dopamine 5 receptor mediates Ang II type 1 receptor degradation via a ubiquitin-proteasome pathway in mice and human cells

Hewang Li,[1] Ines Armando,[1] Peiying Yu,[1] Crisanto Escano,[1] Susette C. Mueller,[2] Laureano Asico,[1] Annabelle Pascua,[1] Quansheng Lu,[1] Xiaoyan Wang,[1] Van Anthony M. Villar,[1] John E. Jones,[1] Zheng Wang,[1] Ammasi Periasamy,[3] Yuen-Sum Lau,[4] Patricio Soares-da-Silva,[5] Karen Creswell,[6] Gaétan Guillemette,[7] David R. Sibley,[8] Gilbert Eisner,[9] Robin A. Felder,[10] and Pedro A. Jose[1]

[1]Department of Pediatrics and [2]Department of Oncology, Lombardi Comprehensive Cancer Center, Georgetown University Medical Center, Washington, DC, USA. [3]Keck Center for Cellular Imaging and Biology Department, University of Virginia, Charlottesville, Virginia, USA. [4]Department of Pharmacological and Pharmaceutical Sciences, College of Pharmacy, University of Houston, Houston, Texas, USA. [5]Institute of Pharmacology and Therapeutics, Faculty of Medicine of Porto, Porto, Portugal. [6]Flow Cytometry and Cell Sorting Center, Lombardi Comprehensive Cancer Center, Georgetown University Medical Center, Washington, DC, USA. [7]Department of Pharmacology, Faculty of Medicine and Health Sciences, Université de Sherbrooke, Sherbrooke, Quebec, Canada. [8]Molecular Neuropharmacology Section, National Institute of Neurological Disorders and Stroke (NINDS), NIH, Bethesda, Maryland, USA. [9]Department of Medicine, Georgetown University Medical Center, Washington, DC, USA. [10]Department of Pathology, University of Virginia Health Sciences Center, Charlottesville, Virginia, USA.

Hypertension is a multigenic disorder in which abnormal counterregulation between dopamine and Ang II plays a role. Recent studies suggest that this counterregulation results, at least in part, from regulation of the expression of both the antihypertensive dopamine 5 receptor (D_5R) and the prohypertensive Ang II type 1 receptor (AT_1R). In this report, we investigated the in vivo and in vitro interaction between these GPCRs. Disruption of the gene encoding D_5R in mice increased both blood pressure and AT_1R protein expression, and the increase in blood pressure was reversed by AT_1R blockade. Activation of D_5R increased the degradation of glycosylated AT_1R in proteasomes in HEK cells and human renal proximal tubule cells heterologously and endogenously expressing human AT_1R and D_5R. Confocal microscopy, Förster/fluorescence resonance energy transfer microscopy, and fluorescence lifetime imaging microscopy revealed that activation of D_5R initiated ubiquitination of the glycosylated AT_1R at the plasma membrane. The regulated degradation of AT_1R via a ubiquitin/proteasome pathway by activation of D_5R provides what we believe to be a novel mechanism whereby blood pressure can be regulated by the interaction of 2 counterregulatory GPCRs. Our results therefore suggest that treatments for hypertension might be optimized by designing compounds that can target the AT_1R and the D_5R.

Introduction

Hypertension is associated with sodium retention caused by decreased renal sodium excretion, which is tightly regulated by both natriuretic and antinatriuretic hormones. Dopamine and Ang II are among those hormones that have counterregulatory effects on cellular signal transduction, production of reactive oxygen species, renal sodium excretion, and blood pressure via renal dopamine D_1-like receptors (dopamine 1 receptor [D_1R] and D_5R subtypes), D_2-like receptors (D_2R, D_3R, and D_4R subtypes), and Ang II type 1 receptors (AT_1Rs) (1–4). The D_5R is widely expressed in the rodent kidney, specifically in the proximal and distal tubules, cortical collecting ducts, medullary ascending limbs of Henle, and arterioles, but not in the glomeruli, juxtaglomerular cells, or macula densa (5). The AT_1R is also widely expressed in the kidney, specifically in the proximal and distal tubules, cortical

collecting ducts, medullary ascending limbs of Henle, arterioles, glomeruli, juxtaglomerular cells, and macula densa (2, 6–8).
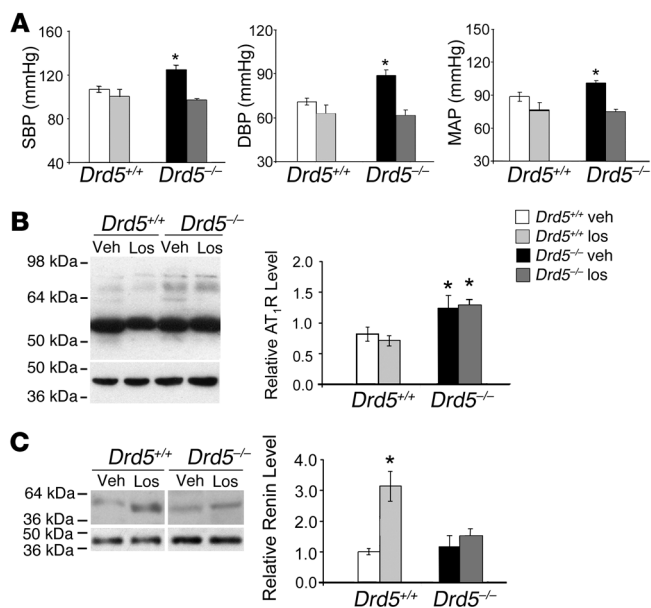
Recent evidence shows that fenoldopam (Fen), a D_1-like receptor agonist, decreases AT_1R protein expression in rat renal proximal tubules (RPTs) and in vascular smooth muscle cells (9). Gene knockdown studies using antisense oligonucleotides that target either the D_1R or D_5R transcript point to D_5R, not D_1R, as the negative regulator of AT_1R protein expression in human RPT cells (10). Furthermore, renal AT_1R protein expression is greater in D_5R knockout ($Drd5^{-/-}$) mice than in wild-type ($Drd5^{+/+}$) littermates (9), and renal D_5R protein expression is increased in $Agtr1a^{-/-}$ mice, underscoring the important downregulatory function of D_5R on AT_1R protein expression, and vice versa. Moreover, $Drd5^{-/-}$ mice are hypertensive and salt sensitive (11), while $Agtr1a^{-/-}$ mice have decreased blood pressure (12), indicating the importance of dopamine receptors (5) and regulators (e.g., GPCR kinase 4; ref. 13) in the regulation of blood pressure.

In this report, we investigated the in vivo and in vitro interaction between D_5R and AT_1R and explored the mechanisms involved in this interaction. We showed that the high blood pressure of $Drd5^{-/-}$ mice, which was associated with increased AT_1R protein expression, was normalized by AT_1R blockade. Activation of the D_5R decreased AT_1R protein level by increasing AT_1R degradation

---

Figure 1
Effect of the AT_1R antagonist losartan on blood pressure and AT_1R and renin protein expression in $Drd5^{+/+}$ and $Drd5^{-/-}$ mice. Vehicle (Veh) or losartan (Los) was administered via intraperitoneal injection every day for 5–7 days in 6-month-old mice. (**A**) Blood pressure was measured directly via the femoral artery under pentobarbital anesthesia. Losartan decreased blood pressure in $Drd5^{-/-}$ but not $Drd5^{+/+}$ mice. SBP, systolic blood pressure; DBP, diastolic blood pressure; MAP, mean arterial pressure. $n = 7$. *$P < 0.05$ versus all other groups, factorial ANOVA, Holm-Sidak test. (**B** and **C**) Whole homogenates (30 μg) of kidneys isolated from **A** were electrophoresed (SDS-PAGE gel) and immunoblotted with anti-AT_1R (**B**) or anti-renin (**C**) antibody. Amounts of glycosylated AT_1R and renin proteins relative to actin were quantified by densitometry. The lanes for the renin blot were run on the same gel but were noncontiguous. $n = 3–5$. *$P < 0.05$ versus vehicle-treated $Drd5^{+/+}$, factorial ANOVA, Holm-Sidak test. Data are mean ± SEM.

in proteasomes via a ubiquitin/proteasome pathway; the degrading action was initiated by the ubiquitination of the glycosylated AT_1R at the plasma membrane. Stimulation of the D_5R dissociated the interaction of the D_5R with the AT_1R and increased the proteasomal degradation of the ubiquitinated AT_1Rs. We believe our results demonstrate a novel paradigm of GPCR-mediated cellular responses and regulation of degradation of one GPCR by another and moreover provide a novel mechanism for the regulation of blood pressure by the dopaminergic system.

Results

Elevated blood pressure in $Drd5^{-/-}$ mice is normalized by an AT_1R antagonist. To test whether the increased expression of the AT_1R in the absence of the D_5R is functionally significant, $Drd5^{+/+}$ and $Drd5^{-/-}$ mice were treated via intraperitoneal injection with vehicle or the AT_1R antagonist losartan daily for 5–7 days. Consistent with previous observations (9, 11), both blood pressure (Figure 1A) and AT_1R protein expression (Figure 1B) were significantly increased in $Drd5^{-/-}$ mice relative to $Drd5^{+/+}$ littermates ($n = 7$; $P < 0.01$). Radioligand binding autoradiography showed that AT_1R expression increased in the renal cortical tubules but not in the glomeruli of $Drd5^{-/-}$ mice (Supplemental Table 1; supplemental material available online with this article; doi:10.1172/JCI33637DS1). Losartan did not change AT_1R protein expression in either $Drd5^{+/+}$ or $Drd5^{-/-}$ mice (Figure 1B), but it decreased blood pressure (systolic, diastolic, and mean arterial pressures) in $Drd5^{-/-}$ but not $Drd5^{+/+}$ mice (Figure 1A), which indicates that the lack of the D_5R increases the effect of the AT_1R on blood pressure and that increased expression of the AT_1R, among other factors, is important in the pathogenesis and maintenance of hypertension in $Drd5^{-/-}$ mice.

We next investigated whether renin, another component of the renin-angiotensin system (RAS), was altered in $Drd5^{-/-}$ mice. As shown in Figure 1C, renal renin protein expression was not significantly altered in $Drd5^{-/-}$ mice compared with their $Drd5^{+/+}$ littermates. As expected, losartan increased renal renin protein expression in $Drd5^{+/+}$ mice ($n = 3–5$; $P < 0.01$); this effect was not observed in $Drd5^{-/-}$ mice ($n = 3–5$; $P = 0.307$).

Elevated blood pressure in $Drd5^{-/-}$ mice is not associated with alterations in renal or plasma catecholamines. We previously reported that high blood pressure of anesthetized $Drd5^{-/-}$ mice was, at least in part, due to increased central nervous sympathetic tone, based on the greater percentage reduction in blood pressure with α_2-adrenergic blockade but similar percentage reduction in blood pressure after adrenalectomy in $Drd5^{-/-}$ mice relative to their wild-type littermates (11). Here, renal and plasma levels of norepinephrine, epinephrine, and L-DOPA were not different between the 2 mouse strains (Supplemental Table 2). However, the renal dopamine level increased in $Drd5^{-/-}$ mice relative to their wild-type littermates (Supplemental Table 2). Therefore, the elevated blood pressure in $Drd5^{-/-}$ mice was not caused by increased peripheral catecholamines or a deficiency in renal dopamine levels.

Activation of D_5R decreases AT_1R protein expression in vitro. Renal crosstransplantation experiments have previously shown that the kidney contributes about 50% of blood pressure regulation (14). The RPT and thick ascending limb of Henle are the sites of increased sodium reabsorption in human essential polygenic hypertension (15), whereas the distal nephron is the site of increased sodium transport in monogenic hypertension (16). Therefore, we next studied the effect of D_1-like receptor stimulation on AT_1R protein expression in human RPT cells, which endogenously expressed D_1R (data not shown), D_5R (Supplemental Figure 2), and AT_1R (Supplemental Figure 2). In human RPT cells, Fen (1 μM for 20 min) decreased AT_1R protein expression (Figure 2). The effect of Fen on AT_1R protein expression was observed for the approximately 70–90 kDa band, but not for the approximately 40–60 kDa band; presumably, the former represents the glycosylated form of AT_1R (17, 18). The observed change in AT_1R expression was specifically caused by D_1-like receptor stimulation, because cotreatment with SCH23390, a D_1-like receptor antagonist that had no effect by itself, abrogated the decrease in AT_1R protein expression (Figure 2). These data indicate that a D_1-like receptor, presumably the D_5R (9, 10), negatively regulates AT_1R protein expression in human RPT cells.

There are no pharmacological reagents that can distinguish the 2 subtypes of D_1-like receptors, D_1R and D_5R (1, 19). Therefore, we transfected D_5R into HEK293 cells, which express no endogenous
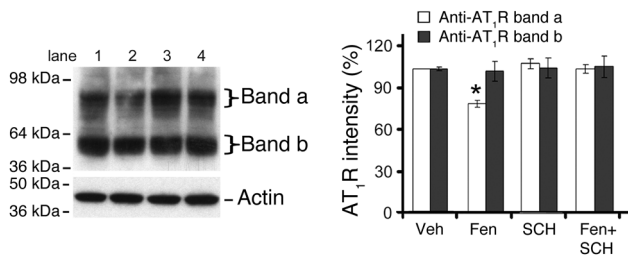
Figure 2
Effect of Fen on AT$_1$R protein expression. Immortalized human RPT cells were incubated with vehicle (lane 1), Fen (1 μM for 20 min; lane 2), or SCH 23390 (1 μM for 50 min) in the absence (lane 3) or presence (lane 4) of Fen. AT$_1$R protein expression in total cell lysates was determined by immunoblotting with anti-AT$_1$R (top panel): 2 bands were observed, denoted a and b, which presumably represent the glycosylated and nonglycosylated forms of the AT$_1$R, respectively (17, 18). Immunoblotting for actin (bottom panel) showed equal sample loading in each lane. Shown is 1 immunoblot from 3 experiments. The effect of vehicle, Fen, or SCH 23390 in the presence or absence of Fen on AT$_1$R protein expression was also quantified. $n = 3$. *$P < 0.05$ versus vehicle, ANOVA, Student-Newman-Keuls test. Data are mean ± SEM.

dopamine receptors (20, 21). To investigate the mechanism of the regulation of AT$_1$R protein expression by the D$_5$R, we transfected human full-length AT$_1$R tagged at the C terminus with EGFP into HEK293 cells expressing the D$_5$R. Flow cytometry (Supplemental Figure 1A) and immunoblot analyses (Supplemental Figure 1B) of the AT$_1$R-EGFP transfectants confirmed the stable heterologous expression of AT$_1$R-EGFP in D$_5$R HEK293 cells. Radioligand binding assays (Supplemental Figure 1C) using ^{3}H-SCH 23390 and ^{125}I-Sar^1 Ang II as ligands for the D$_1$-like receptors (here, only the D$_5$R) and the AT$_1$R, respectively, also showed the expression of both the D$_5$R and the AT$_1$R. Ang II increased the phosphorylation of ERK1/2 in a dose-dependent manner (Supplemental Figure 1D), indicating that the EGFP tag did not impair AT$_1$R function in the transfected cells.

We next tested whether activation of the D$_5$R decreased AT$_1$R protein expression in the transfected cells (designated AT$_1$R/D$_5$R HEK293 cells). Fen decreased the approximately 100–120 kDa band, which presumably represents the glycosylated AT$_1$R plus the EGFP tag, but not the approximately 65–85 kDa AT$_1$R band, which presumably represents the nonglycosylated AT$_1$R plus the EGFP tag, as early as 20 minutes after treatment (Figure 3A). Because the D$_1$R is not expressed in HEK293 cells (20, 21), these results indicate that the effect of Fen on AT$_1$R protein expression is solely the result of D$_5$R activation.

Treatment with PNGase F (Figure 3B) greatly decreased the intensity of the approximately 100–120 kDa AT$_1$R band, which indicates that this band represents the glycosylated form of the receptor. Thus, the D$_5$R

only affects the expression of the glycosylated species of AT$_1$R. Moreover, the rapid D$_5$R-mediated decrease of this band, but not the approximately 65–85 kDa AT$_1$R band (Figure 3A), indicates that the inhibitory effect does not result from the downregulation of transcription or translation, but rather may be the result of increased AT$_1$R protein degradation.

Characterization of D$_5$R-mediated AT$_1$R degradation. To characterize the D$_5$R-mediated AT$_1$R turnover, we performed pulse-chase experiments by [^{35}S] methionine/cysteine (Met/Cys) labeling of AT$_1$R/D$_5$R HEK293 cells treated with vehicle, Fen, or Ang II. Stimulation of the D$_5$R with Fen resulted in degradation of the AT$_1$R more rapid than that observed with vehicle treatment, but slower than that with Ang II treatment (Figure 4). Unlike Ang II, which increased degradation of both the glycosylated and the nonglycosylated AT$_1$R, Fen increased the degradation of only the glycosylated AT$_1$R (Figure 4A), and the amount of the approximately 100–120 kDa AT$_1$R band decreased as a function of time ($0.365 + 0.618^{-t/22.2}$), which suggests a first-order decay.

Protein degradation in mammalian cells occurs primarily in either lysosomes or proteasomes (22, 23). Spontaneous or Ang II–induced AT$_1$R degradation occurs in lysosomes (24, 25). To explore the sites of D$_5$R-mediated AT$_1$R degradation in AT$_1$R/D$_5$R HEK293 cells, we examined the colocalization of the AT$_1$R with marker proteins for proteasomes or lysosomes using laser scanning confocal microscopy. Under basal conditions, a substantial fraction of AT$_1$Rs (43.47%) were localized at the plasma membrane (Supplemental Figure 3 and Supplemental Table 3), consistent with the previous observation that the mouse AT$_{1A}$R mainly localizes at
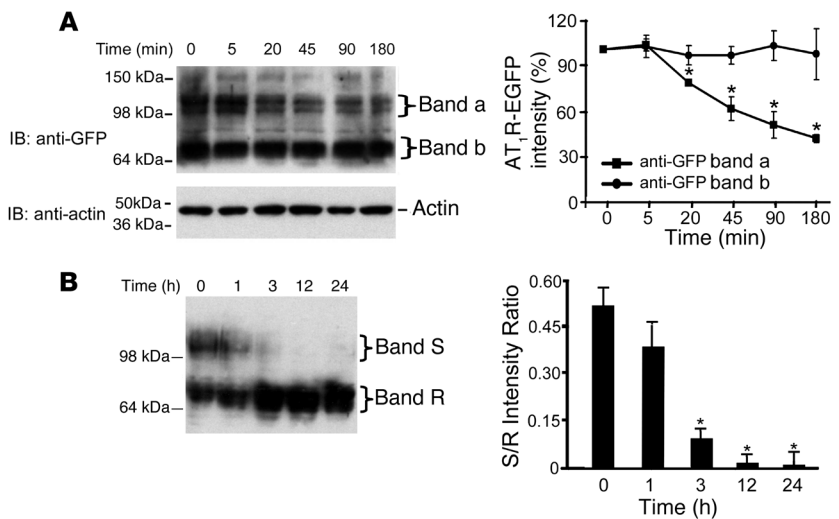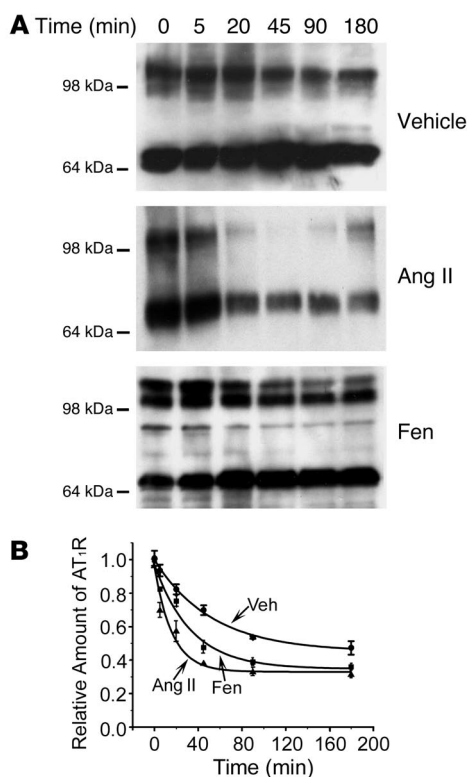

Figure 3
Effect of D$_5$R stimulation on the expression of the glycosylated form of the AT$_1$R protein. (**A**) AT$_1$R/D$_5$R HEK293 cells were incubated with Fen (1 μM) for the indicated times; total cell lysates were electrophoretically separated, transferred onto nitrocellulose membranes, and immunoblotted with anti-GFP (band a, ~100–120 kDa; band b, ~65–85 kDa) to detect AT$_1$R protein expression. Immunoblotting for actin was used to monitor the sample protein loading. $n = 3$. *$P < 0.05$ versus 0 min, ANOVA, Student-Newman-Keuls test. (**B**) Protein samples (50 μg) from AT$_1$R/D$_5$R HEK293 cells were incubated with 10 mU PNGase F at 37°C for the indicated times, electrophoretically separated, transferred onto nitrocellulose membranes, and immunoblotted with anti-GFP antibody. Band S is sensitive to PNGase F and corresponds to the glycosylated form of the AT$_1$R (band a). Band R is resistant to PNGase F and corresponds to the nonglycosylated form of the AT$_1$R (band b). The ratio of band S intensity to band R intensity was determined by densitometry in 3 separate experiments. $n = 3$. *$P < 0.05$ versus 0 h, ANOVA, Student-Newman-Keuls test. Data are mean ± SEM.

Figure 4
Characterization of AT_1R degradation by $[^{35}S]$ metabolic labeling. AT_1R/D_5R HEK293 cells were treated with vehicle, Ang II (100 nM for 30 min), or Fen (1 μM for 2 h), pulsed with $[^{35}S]$ Met/Cys, and then chased with cold amino acids for the indicated times. The cell lysates were immunoprecipitated with anti-GFP antibody, and the immunocomplexes were subjected to SDS-PAGE. Dried gels were exposed to X-ray films. (**A**) Autoradiographs of AT_1R degradation with vehicle, Ang II, and Fen treatment. (**B**) Quantification of AT_1R degradation. Values are mean ± SEM of arbitrary density units normalized to the time-0 value ($n = 3$). The decrease in AT_1R protein in the presence of vehicle followed a first-order exponential curve, with a half-life of 127.6 min. The decrease in AT_1R protein with Ang II or Fen treatment also followed a first-order exponential curve; treatment with Ang II decreased the half-life of AT_1R protein to 16.8 min, while treatment with Fen resulted in a half-life of 37.7 min. $P < 0.05$, Fen versus vehicle and versus Ang II, repeated-measures ANOVA. No error bar is visible when the SEM is smaller than the symbol.

the plasma membrane (26). Lysosome-associated membrane protein 1 (LAMP 1), a marker of lysosomes, and $p44S^{10}$, a marker of proteasomes, were scattered throughout the cytoplasm with much less expression at the plasma membrane (Supplemental Figure 3). In the cytoplasm, there was some colocalization of the AT_1R and LAMP 1 (23.19%) and of the AT_1R and $p44S^{10}$, albeit to a lesser degree (11.26%; Supplemental Figure 3 and Supplemental Table 4). Stimulation with Fen resulted in considerable internalization of AT_1Rs with patches and clusters of AT_1R fluorescence in both plasma membrane and cytoplasm. Fen treatment increased the colocalization of AT_1R with $p44S^{10}$ from 11.26% to 56.12%, whereas the treatment did not affect the percentage of colocalization between AT_1Rs and LAMP 1 (Supplemental Figure 3 and Supplemental Table 4). In contrast, treatment with Ang II increased the colocalization between AT_1Rs and LAMP 1 without affecting that between AT_1R and $p44S^{10}$ (Supplemental Figure 3). These results strongly suggest that upon activation, the D_5R directs the degradation of the AT_1R to proteasomes and not to lysosomes. The Fen-induced changes in the intracellular distribution of the AT_1R did not occur in the cells incubated with SCH23390 prior to Fen treatment (Supplemental Figure 3 and Supplemental Tables 3 and 4), which indicates that the effect of Fen was through the activation of the D_5R.

D_5R-mediated AT_1R degradation occurs in proteasomes, but not lysosomes. To investigate further the D_5R-mediated AT_1R degradation in AT_1R/D_5R HEK293 cells, we used clasto-lactocystin β-lactone (CLBL), a proteasome inhibitor, and chloroquine (Chlor), a lysosome inhibitor, in $[^{35}S]$ Met/Cys metabolic experiments. Fen-stimulated AT_1R degradation was greatly reduced in the presence of CLBL but not Chlor; the half-life of the AT_1R in the presence of CLBL was 149.5 min (decay rate, 0.537), while it was 43.8 min (decay rate, 0.665) in the presence of Chlor (Fig-

ure 5A). Morphological observation showed that CLBL, but not Chlor, abrogated the Fen-stimulated colocalization of AT_1R and $p44S^{10}$ (Figure 5B and Supplemental Table 4). In the presence of CLBL, image analysis showed that 42.40% of AT_1R resided in the plasma membrane in spite of the presence of Fen (Supplemental Table 3). Flow cytometry data also showed that CLBL, but not Chlor, inhibited the Fen-stimulated degradation of the AT_1R (Figure 5C). Chlor alone slightly increased the AT_1R fluorescence (Figure 5C), consistent with previous observations that spontaneous degradation of the AT_1R occurs in lysosomes (24, 25). Again, inhibition of proteasome but not lysosome activity abrogated D_5R-mediated AT_1R degradation, which confirmed that this degradation occurs in proteasomes.

To corroborate the biochemical and morphological studies indicating that exogenously and endogenously expressed AT_1Rs are directed to proteasomes after Fen stimulation, proteasomes were isolated from human RPT cells treated with vehicle, Ang II, or Fen. Using proteasome affinity beads, AT_1Rs were identified in proteasomes isolated from Fen-treated human RPT cells, but not in those isolated from vehicle- and Ang II–treated cells (Figure 5D), which indicates that Fen stimulation directs endogenously expressed AT_1R to proteasomes in human RPT cells.

AT_1R interacts with ubiquitin and is ubiquitinated at the plasma membrane. Ubiquitin (Ub) modification plays an important role in targeting proteins for degradation (23, 27–32). To determine the role of ubiquitination in the degradation of the AT_1R, we first studied the colocalization of Ub (and ubiquitinated proteins), $p44S^{10}$, and the AT_1R in vehicle- and Fen-treated cells (Figure 6A). In vehicle-treated cells, Ub and $p44S^{10}$ were scattered throughout the cytoplasm, and minimal — if any — colocalization was observed among the 3 proteins (Figure 6A). In contrast, Fen treatment induced significant colocalization of the AT_1R and $p44S^{10}$, the AT_1R and Ub, Ub and $p44S^{10}$, and the AT_1R, Ub, and $p44S^{10}$ at the plasma membrane (Figure 6A and Supplemental Table 5).

To validate the morphological findings observed with confocal microscopy, Förster/fluorescence resonance energy transfer (FRET) microcopy (33) was used to detect the interaction between the AT_1R and endogenous Ub in AT_1R/D_5R HEK293 cells. Fen stimulation markedly increased the energy transfer of the AT_1R and Ub at the plasma membrane from 3.6% ± 1.2% in unstimulated cells to 34.1% ± 2.4% (Figure 6B). At the same time, the energy
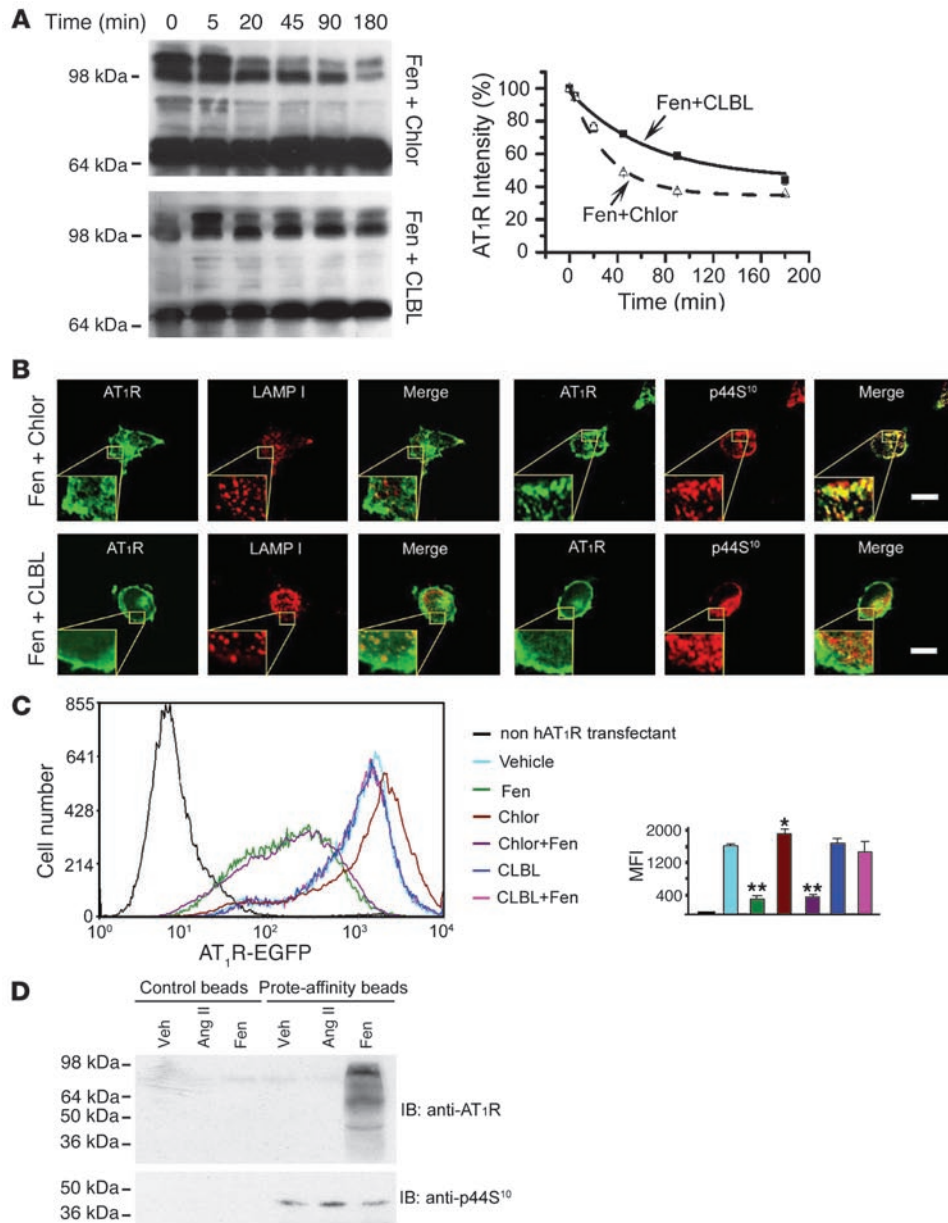
Figure 5
Fen-stimulated AT_1R degradation occurs in proteasomes but not lysosomes. (**A**) AT_1R/D_5R HEK293 cells treated with Fen (1 μM for 2 h) and either Chlor (100 μM for 3 h) or CLBL (4 μM for 3 h) were pulsed with [^{35}S] Met/Cys and chased with cold amino acids for the indicated times. Shown is 1 autoradiograph of each treatment. Data (mean ± SEM) followed a first-order exponential curve for both treatments. The AT_1R protein half-life was 43.8 min for Fen plus Chlor and 149.5 min for Fen plus CLBL. $n = 3$. (**B**) Subcellular distribution of AT_1R in AT_1R/D_5R HEK293 cells treated as in **A**. Green, AT_1R-EGFP; red, lysosomes or proteasomes (detected by Alexa Fluor 633–conjugated anti–LAMP 1 or anti-p44S^{10}); yellow, colocalization. Scale bars: 10 μm; 2.5 μm (insets). (**C**) AT_1R/D_5R HEK293 cells were treated with vehicle, Fen (1 μM for 6 h), Chlor (100 μM for 10 h), CLBL (4 μM for 10 h), Chlor plus Fen, or CLBL plus Fen. Nontransfected D_5R HEK293 cells are shown as a control. Right: MFI of AT_1R-EGFP. $n = 3$. *$P < 0.05$, **$P < 0.001$ versus vehicle, ANOVA, Student-Newman-Keuls test. Data are mean ± SEM. (**D**) Human RPT cells were treated with vehicle, Ang II, or Fen; cell lysates were incubated with control or proteasome-affinity beads for 4 hours at 4°C. After washing, the matrix was suspended in SDS sample buffer, separated by SDS-PAGE, and transferred onto nitrocellulose. Membranes were immunoblotted for either AT_1R or p44S^{10}. Experiments were repeated twice with similar results.

transfer had no obvious increase in the cytoplasm, which indicates that Fen stimulation increased the AT_1R and Ub interaction initially at the plasma membrane but not in the cytoplasm.

Fluorescence lifetime imaging microscopy (FLIM) allows quantitative monitoring of protein interaction by measuring the change in lifetime of the donor molecule, which does not require any spectral bleed-through correction and is independent of change in fluorophore concentration and excitation intensity (34). To verify the above observations obtained with FRET microscopy, FLIM was used to measure the interaction between the AT_1R and Ub at the plasma membrane by monitoring the quench time (τ) of the AT_1R (as a donor) in the presence or absence of Ub (as an acceptor). As shown in Figure 7A, the average τ_m of the AT_1R was 2.32 ns in the absence of the acceptor and 2.33 ns in vehicle-treated cells in the presence of the acceptor. Fen stimulation shortened the average τ_1 of the AT_1R to 1.68 ns

because of the occurrence of FRET between the AT_1R and Ub, which suggests their interaction upon Fen stimulation. There was no interaction between them in the basal state, consistent with the confocal and FRET microscopy observations.

To determine directly whether the AT_1R is ubiquitinated, human RPT (Figure 7B) and AT_1R/D_5R HEK293 (Supplemental Figure 4) plasma membrane fractions were isolated by biotinylation, immunoprecipitated with anti-AT_1R or anti-GFP, and immunoblotted with Ub antibody (clone FK1). Fen caused the polyubiquitination of both endogenous (Figure 7B) and heterologously overexpressed (Supplemental Figure 4) AT_1R, which was not observed in the basal state. The Fen-stimulated ubiquitination of AT_1R was similar in the presence (RPT cells) or absence (AT_1R/D_5R HEK293 cells) of the D_1R, which indicates that the D_1R was not involved in D_5R-mediated AT_1R ubiquitination. The Fen-stimulated polyubiquitination of the endogenous AT_1R was
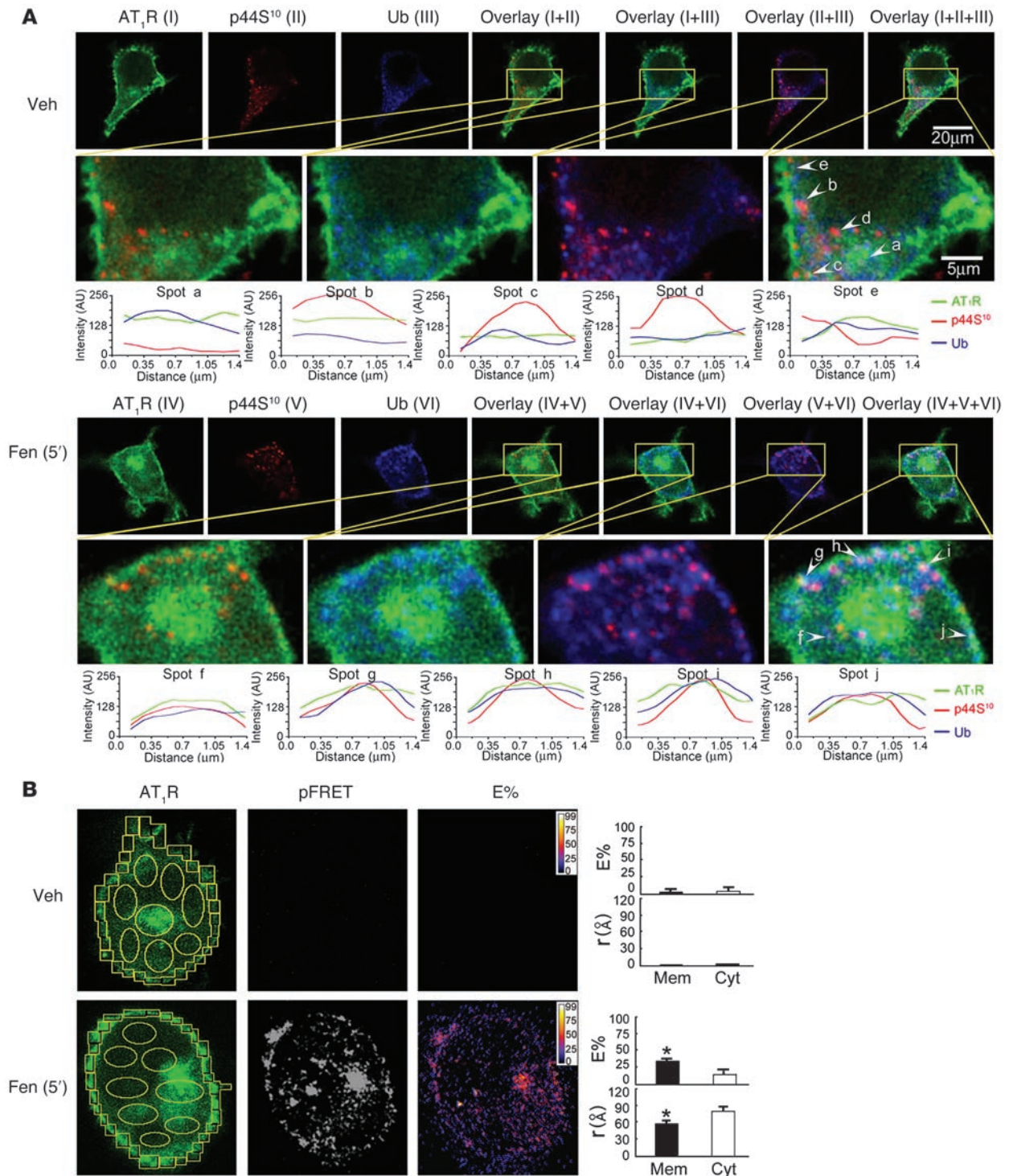
Figure 6

The AT$_1$R is ubiquitinated, and the ubiquitination of the AT$_1$R is initiated at the plasma membrane. AT$_1$R/D$_5$R HEK293 cells were treated with vehicle or Fen (1 μM for 5 min). (**A**) Immunostaining for p44S[10] or Ub (clone P4D1). Distance calibration was based on objective and zoom of the images taken: 1 pixel equals 0.133 μm. Green, EGFP-tagged AT$_1$R; red, p44S[10]; blue, Ub; yellow, colocalization of AT$_1$R and p44S[10] (green and red); cyan, colocalization of AT$_1$R and Ub (green and blue); magenta, colocalization of p44S[10] and Ub (red and blue); white, colocalization of AT$_1$R, Ub, and p44S[10] (red, green, and blue). Scale bars shown for vehicle-treated cells also apply to Fen-treated cells. (**B**) The image of AT$_1$R-EGFP (as donor fluorophore) was used for drawing ROIs, which were divided into plasma membrane (rectangles) and cytoplasm (ovals) to determine the spatial interaction between the AT$_1$R and Ub (clone P4D1, Alexa Fluor 555; as acceptor fluorophore). The pure FRET and 2-dimensional distribution images of energy transfer efficiency (E%) were generated as described in Methods. Graphs show mean ± SEM energy transfer efficiency and distance (r) of ROIs in the plasma membrane (Mem) and cytoplasm (Cyt) in the corresponding AT$_1$R images processed from 6–8 cells. *$P < 0.05$ versus vehicle, Student's t test. Distances beyond experimental limitations (>90 Å) are given a 0 value, indicating no occurrence of FRET.
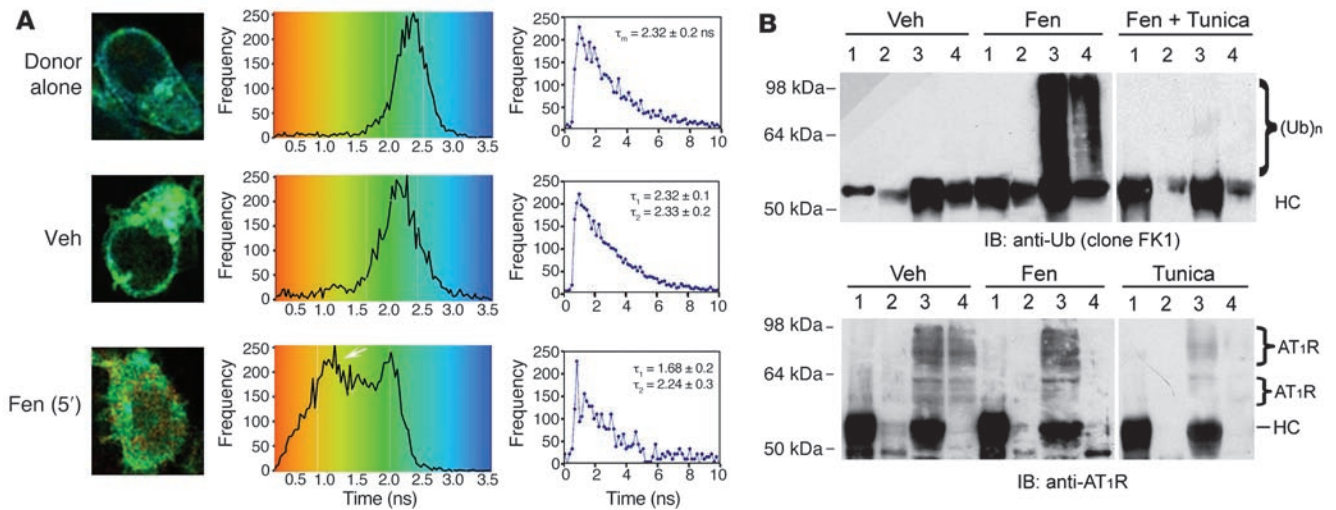
Figure 7
Glycosylation is necessary for the ubiquitination of AT_1R at the plasma membrane. (**A**) AT_1R/D_5R HEK 293 cells were treated with vehicle or Fen (1 μM for 5 min). Shown are FLIM images, histograms, and decay graphs of cells treated in the absence (top) or presence (middle and bottom) of acceptor (Ub). The left shift (arrow) of AT_1R lifetime in Fen-treated samples demonstrated the occurrence of FRET. The lifetime of AT_1R (donor) in the absence of acceptor was 2.32 ± 0.2 ns; it was 2.33 ± 0.2 ns in the presence of acceptor with vehicle treatment, indicating no energy transfer. With Fen treatment in the presence of acceptor, the donor lifetime had 2 peaks: the first was quenched at 1.68 ± 0.2 ns (τ_1) because of the occurrence of FRET, with a corresponding energy transfer efficiency of 27.6% ± 3.7%; the second was 2.24 ± 0.3 ns (τ_2), which represented the unquenched AT_1R. The FLIM patterns observed in the basal state and after Fen were similar in 4 different experiments. Quantification was performed in 16–30 cells from 1 of the 4 experiments. Data are mean ± SEM. (**B**) Human RPT cells were treated with vehicle, Fen (1 μM for 5 min), tunicamycin (Tunica; 10 μg/ml for 12 h), or tunicamycin plus Fen. Cell membrane fractions isolated by biotinylation were immunoprecipitated with normal mouse Ig M/G (lane 1), normal rabbit IgG (lane 2), anti-AT_1R mAb (lane 3), or anti-D_5R antibody (lane 4) and immunoblotted with anti-Ub (clone FK1) or anti-AT_1R mAb. $(Ub)n$, polyubiquitin chain; HC, heavy chain.

prevented by tunicamycin treatment (Figure 7B), indicating that glycosylation of the AT_1R was necessary for its ubiquitination at the plasma membrane. Coimmunoprecipitation of the endogenous AT_1R with the D_5R in vehicle-treated cells, but not in Fen-treated cells, suggested that the AT_1R interacted with the D_5R in the basal, unstimulated state and that Fen dissociated their interaction (Figure 7B). Failure to detect coimmunoprecipitation of the AT_1R with the D_5R after tunicamycin treatment indicated that the interaction of the AT_1R and the D_5R in the basal state required glycosylation of the AT_1R and/or the D_5R.

Discussion
Our results demonstrate what we believe to be a novel mechanism of the regulation of the AT_1R protein expression, which is physiologically important in vivo. The D_5R mediates the degradation of glycosylated AT_1R through the Ub/proteasome pathway, a process initiated at the plasma membrane, in contrast to either spontaneous or Ang II–mediated degradation of the AT_1R, which occurs in lysosomes.

Ubiquitination plays important roles in the regulation of proteins destined for lysosome or proteasome degradation (28, 35). A number of GPCRs in mammalian cells have been reported to be ubiquitinated, such as the β_2-adrenegic receptor (36), chemokine receptor CXCR4 (37, 38), platelet-activating factor receptor (39), and protease-activated receptors 1 and 2 (40, 41). However, to our knowledge, no previous studies have suggested that the AT_1R is ubiquitinated following its stimulation. Indeed, the agonist-mediated endocytosis of the rodent $AT_{1A}R$ does not require ubiquitination of the receptor (42).

Lysine is the target amino acid for ubiquitination. The human AT_1R contains many lysine residues, especially in its intracellular domains: in 19% (10 of 53) of its carboxy terminus, 20% (4 of 20) of its third intracellular loop, 7% (1 of 15) of its second intracellular loop, and 20% (2 of 10) of its first intracellular loop. Even though ubiquitination is not required for rodent $AT_{1A}R$ internalization either in the basal state or following Ang II stimulation in CHO cells (42), human AT_1R ubiquitination can still occur under certain conditions. Our results showed that following short-term D_5R stimulation, Ub accumulated at sites where the AT_1R was located at the plasma membrane (Figure 6, A and B, and Figure 7A), where it was initially ubiquitinated (Figure 7B). The ubiquitinated AT_1Rs were then directed to proteasomes for subsequent degradation (Figures 5–7).

N-glycosylation is a common posttranslational modification of GPCRs and plays roles in the formation of their active conformation, targeting to the cell surface and intracellular signaling (43). Human bradykinin B2 receptor requires N-glycosylation for its maturation at the cell surface (44); certain sites of β_2-adrenergic receptor N-glycosylation can alter receptor targeting to the degradation pathway (45). Both dopamine receptors (46, 47) and the AT_1R (17, 18) are N-glycosylated. Glycosylation is required for the D_5R to be functionally expressed at the cell surface (46). N-glycosylation of the AT_1R is important for its proper folding, targeting, and cell surface display (18). Our results showed that glycosylation was required for the interaction of AT_1R with D_5R (Figure 7B), which is consistent with previous observation that glycosylation is important for their homologous (44) or heterologous (47) interaction with their binding partners to accomplish a series

of intracellular functions. Glycosylation may also serve as a signal for AT_1R ubiquitination upon Fen stimulation and subsequent degradation in proteasomes (refs. 48–50, Figure 7B, and Supplemental Figure 4), which is consistent with a previous observation that N-linked high-mannose oligosaccharides recognized by Ub ligase lead to the ubiquitination of N-glycosylated proteins (49). Therefore, we speculate that ubiquitination of the glycosylated AT_1R expressed at the plasma membrane initiates its degradation in proteasomes (Figures 6 and 7). Additionally, glycosylation may protect the nascent AT_1R from proteolytic degradation (6, 7, 48). However, the protection is superseded by activation of the D_5R, resulting in targeting of the receptor to proteasomes for degradation (Figures 6 and 7).

Both the D_5R and the AT_1R are GPCRs that are important in the regulation of sodium balance and blood pressure. The RAS regulates blood pressure by renal and nonrenal mechanisms (2, 6, 7, 14, 51). The paracrine regulation of sodium transport in the proximal tubule by the RAS is exerted via several angiotensin receptor subtypes (AT_1R, AT_2R, and AT_4R) (2, 6, 7). The activation of AT_1Rs by Ang II increases sodium transport, whereas the activation of AT_2R and AT_4R decreases sodium reabsorption. Under physiologic conditions, the major effect of Ang II is to stimulate sodium transport via the AT_1R (2, 6, 7). In the hypertensive state, the AT_1R function is increased, which may or may not be associated with increased expression (2, 6–8). However, the mechanism underlying this phenomenon in RPTs is not completely clear. Assessment of the in vivo expression levels of D_5R and AT_1R following dopaminergic or AT_1R stimulation may clarify this issue. Dopamine and its receptors have been reported to participate in the regulation of the RAS, including Ang II receptors (5, 9, 52, 53). D_1-like receptors have been reported to increase the AT_2R (53) and decrease the AT_1R (9, 52) expression in RPTs. The D_1-like receptor subtype regulating the expression of a particular angiotensin receptor subtype has not been established.

Second-generation $Drd5^{-/-}$ mice in a mixed B129Sv and C57BL/6 background (11, 21) and F6 $Drd5^{-/-}$ mice in a C57BL/6 (>98% congenic) background (9, 21) have high blood pressure (9, 11, 21) and increased AT_1R protein expression (9). Renal or plasma catecholamine levels (Supplemental Table 2) could not explain the increased blood pressure and AT_1R protein expression observed in $Drd5^{-/-}$ mice. Renal renin protein expression was not different between $Drd5^{-/-}$ and $Drd5^{+/+}$ littermates (Figure 1C). Renin is mainly synthesized and secreted by juxtaglomerular cells, which express AT_1R and D_1R, but not D_5R (11). Because D_5R is not expressed in juxtaglomerular cells, one would expect no change in AT_1R expression or alteration in renin levels via the AT_1R/renin feedback loop. Although D_1R can increase renin secretion, D_1R protein expression in the brain and kidney is not altered by knocking out the gene encoding D_5R (11). This indicates that the juxtaglomerular AT_1R/renin feedback loop is not altered by knocking out the D_5R gene. Consistent with previous reports (54), AT_1R blockade with losartan treatment increased renal renin expression in $Drd5^{+/+}$ mice. Interestingly, this effect was not observed in $Drd5^{-/-}$ mice, the mechanism of which remains to be determined. Nonetheless, our results showed that the increased blood pressure in $Drd5^{-/-}$ mice was probably not caused by increased production of renin and/or Ang II.

The results of the present study show that the hypertension resulting from the absence of the gene encoding D_5R is caused, at least in part, by the increase in AT_1R protein expression, because of the absence of the negative counterregulatory effect of the D_5R

on the AT_1R. Activation of the D_5R initiated AT_1R ubiquitination, which directed the AT_1R to proteasomal degradation (Figures 5–7). Glycosylation was required for the ubiquitination of the AT_1R (Figure 7). These results provide evidence for a mechanism by 2 posttranslational modifications crucial in the regulation of the AT_1R, a class B GPCR, mediated by the D_5R, a class A GPCR. The negative regulation of the AT_1R expression by the D_5R has physiological consequences, because chronic administration of the AT_1R blocker losartan normalized the elevated blood pressure of $Drd5^{-/-}$ mice (Figure 1A). Inhibition of the RAS is an important component of the treatment of essential hypertension, but the control of hypertension remains suboptimal (55). Our results showing that the antihypertensive effect of D_1-like receptors counteracted the prohypertensive effects of the RAS, in part by D_5R-mediated degradation of the AT_1R, provides opportunities for designing specific drugs that can target the AT_1R and/or the D_5R for the optimization of hypertension therapy.

Methods

Antibodies and reagents; cell lines and transfection; radioligand binding; radioligand binding autoradiography; biotinylation and immunoprecipitation; deglycosylation; proteasome isolation; flow cytometry; and determination of catecholamine levels. See Supplemental Methods.

$Drd5^{-/-}$ mice and blood pressure measurement. The animal protocols were reviewed and approved by the Georgetown University Animal Care and Use Committee. For details, see Supplemental Methods.

Pulse-chase. AT_1R/D_5R HEK293 cells were labeled by ^{35}S-labeled Met/Cys as described previously (56). Briefly, cells were starved in Met/Cys-free DMEM (Invitrogen) containing 10% dialyzed FBS for 2 h and pulsed for 3 h with medium containing 300 µCi/ml ^{35}S-labeled Met/Cys. Cycloheximide (10 µg/ml) was added to inhibit de novo protein synthesis and then chased for varying durations in full culture medium containing 3 mM unlabeled Met/Cys. At the end of each individual chase period, the cells were washed with PBS 3 times to remove unbound label. Cell pellets were lysed with lysis buffer, and the AT_1R was immunoprecipitated using anti-GFP antibody. Immunoprecipitated protein complexes were eluted with protein sample buffer at 85°C for 15 minutes and resolved by SDS-PAGE. Dried gels were exposed to X-ray films for autoradiography. The quantified AT_1R bands were normalized to the time-0 value. The mean and SEM of 3 experiments were plotted, and the exponential decays were calculated (OriginPro; OriginLab Corp.). The decay rate constants and the half-lives of the AT_1R protein, which represent the rates of AT_1R degradation, were calculated based on individual decay equations.

Confocal immunofluorescence microscopy. AT_1R/D_5R HEK293 cells were fixed with 4% paraformaldehyde in PBS for 20 min at room temperature. After washing with PBS, the fixed cells on coverslips were incubated overnight at 4°C with Alexa Fluor 633–conjugated (Invitrogen) polyclonal rabbit LAMP 1 (2 µg/ml) or polyclonal goat p44S10 antibody (5 µg/ml), or Alexa Fluor 546–conjugated (Invitrogen) monoclonal mouse Ub antibody (2 µg/ml). Coverslips were mounted in SlowFade mounting medium (Invitrogen) and sealed onto glass slides. Samples were imaged using an Olympus Fluoview FV300 laser scanning confocal microscope equipped with a ×60/1.4 NA objective. Quantitative analysis was conducted by using MetaMorph 6.1 (Molecular Devices). Background was subtracted from each image, after which the images were thresholded to identify specific protein fluorescence. Whole cells, plasma membrane, or cytoplasmic areas were identified by creating regions of interest (ROIs). Fluorescence in each (integrated intensity) was determined and expressed as percent of total fluorescence for cytoplasm and plasma membrane. For determination of colocalization, the function "Colocalization" in MetaMorph software was used where percent overlap

(integrated intensity measurement) was determined for AT_1R over LAMP 1, or AT_1R over $p44S^{10}$, Ub over AT_1R, and Ub over $p44S^{10}$.

FRET microscopy and data processing. The fluorophore pairs used for FRET imaging in this study were AT_1R-EGFP (as donor dipole) and Alexa Fluor 555 (as acceptor dipole; Invitrogen) conjugated with Ub antibody. Seven images were acquired for each FRET analysis, as described previously (33), with an Olympus Fluoview FV300 laser scanning confocal microscope equipped with a ×60/1.4 NA objective, argon (488 nm) and HeNe (543 nm) laser, emission filters 515/50 nm and 590 nm LP. Either single-labeled donor and acceptor samples or double-labeled samples were acquired under the same condition throughout the image collection. The uncorrected FRET images (uFRET) were acquired by donor excitation in acceptor channel, which contained pure FRET (pFRET) and contaminations from both donor and acceptor spectral bleed-through (SBT). pFRET images were generated using a previously described algorithm (33) for pixel-by-pixel removal of donor and acceptor SBT on the basis of matched fluorescence levels between the double-labeled specimen and single-labeled reference specimens.

ROIs were selected in the uFRET images (33). In this study, we used image e (donor excitation in donor channel of double-labeled specimen) as the reference image for selection of ROIs to separate plasma membrane and cytoplasm fluorescence. The percentage of energy transfer (E%) images was processed on a pixel-by-pixel basis by using the equation E% = 1 – {Ida/(Ida + pFRET × [Pd/Pa] × [Sd/Sa] × [Qd/Qa])}; where Pd and Pa (photo multiplier tube gain of donor and acceptor channels, respectively) set to the same when images were acquired; Sd and Sa (spectral sensitivity of donor and acceptor channels, respectively) were provided by the manufacturer; Qd and Qa (donor and acceptor quantum yield, respectively) were measured by spectrofluorometer as described previously (57); Ida is the image of donor excitation in donor channel of double labeling samples after removing of background; and pFRET is the processed or corrected FRET. The calculation of distance of donor and acceptor (r) was based on the following previously described equation (33): $r = R_0\{(1/E)-1\}^{1/6}$, where E is the efficiency of energy transfer. Förster's distance (R_0) in this study was 67.5 (33).

FLIM. Cell preparation and fluorophores of samples were performed as described above. Time-domain FLIM was performed with a 120-s acquisition in a 2-photon BioRad Radiance 2100 microscope with ×60 NA 1.4 objective lens at the M.W. Keck Center for Cellular Imaging of the University of Virginia, as described previously (34). The AT_1R was fused with EGFP as the donor fluorophore, and the acceptor fluorophore was Ub (clone P4D1), conjugated with Alexa Fluor 555. The single exponential decay of lifetime was processed in the donor alone samples, and the double

exponential decay of lifetime was performed in the presence of acceptor fluorophores. Donor fluorophores (AT_1R-EGFP) were excited at 790 nm by a femtosecond pulse from a coherent ti:sapphire laser system. Emissions filtered with a center of 515 nm were collected by a high-speed photomultiplier tube (MCP R3809; Hamamatsu), and fluorescence lifetime imaging capability was incorporated, with addition of a fast time-correlated single photon counting acquisition board (SPC 730; Becker and Hickl). Fluorophore lifetimes were fitted to 1- or 2-exponential decay curves on SpcImage 2.60 (Becker and Hickl). The non-FRETing population, measured as the donor lifetime in the absence of an acceptor, is represented as τ_2; the FRETing population (τ_1) is represented in the figures. The energy transfer efficiency is calculated as $1 - (\tau_{DA}/\tau_D)$, where τ_{DA} and τ_D are the donor excited state lifetimes in the presence and absence, respectively, of the acceptor. Cell images and lifetime distributions are representative examples. The FLIM patterns observed in the basal state and after Fen were similar in 4 different experiments. Quantification was performed in 16–30 cells from 1 of the 4 experiments.

Statistics. Results are expressed as mean ± SD or SEM as indicated. Significant differences among groups were determined by factorial or repeated ANOVA (Holm-Sidak or Student-Newman-Keuls test) for multiple comparisons and Student's t test for 2 comparisons. $P < 0.05$ was considered statistically significant (SigmaStat 3.0; SPSS Inc.).

1. Jose, P.A., Eisner, G.M., and Felder, R.A. 1998. The renal dopamine receptors in health and hypertension. *Pharmacol. Ther.* **80**:149–182.
2. de Gasparo, M., Catt, K.J., Inagami, T., Wright, J.W., and Unger, T. 2000. International union of pharmacology. XXIII. The angiotensin II receptors. *Pharmacol. Rev.* **52**:415–472.
3. Efendiev, R., et al. 2003. Intracellular Na^+ regulates dopamine and angiotensin II receptors availability at the plasma membrane and their cellular responses in renal epithelia. *J. Biol. Chem.* **278**:28719–28726.
4. Hussain, T., and Lokhandwala, M.F. 2003. Renal dopamine receptors and hypertension. *Exp. Biol. Med.* **228**:134–142.
5. Zeng, C., et al. 2008. Dysregulation of dopamine-dependent mechanisms as a determinant of hypertension: studies in dopamine receptor knockout mice. *Am. J. Physiol. Heart Circ. Physiol.* **294**:H551–H569.
6. Kobori, H., Nangaku, M., Navar, L.G., and Nishiyama, A. 2007. The intrarenal renin-angiotensin system: from physiology to the pathobiology of hypertension and kidney disease. *Pharmacol. Rev.* **59**:251–287.
7. Paul, M., Poyan-Mehr, A., and Kreutz, R. 2006. Physiology of local renin-angiotensin systems. *Physiol. Rev.* **86**:747–803.
8. Hall, J.E., Brands, M.W., and Henegar, J.R. 1999. Angiotensin II and long-term arterial pressure regulation: the overriding dominance of the kidney. *J. Am. Soc. Nephrol.* **10**:S258–S265.
9. Zeng, C., et al. 2005. Interaction of angiotensin II type 1 and D_5 dopamine receptors in renal proximal tubule cells. *Hypertension.* **45**:804–810.
10. Felder, R.A., et al. 2003. Human renal angiotensin type 1 receptor regulation by the D1 dopamine receptor [abstract]. *Hypertension.* **42**:438.
11. Hollon, T.R., et al. 2002. Mice lacking D5 dopamine receptors have increased sympathetic tone and are hypertensive. *J. Neurosci.* **22**:10801–10810.
12. Mangrum, A.J., Gomez, R.A., and Norwood, V.F. 2002. Effects of AT_{1A} receptor deletion on blood pressure and sodium excretion during altered dietary salt intake. *Am. J. Physiol. Renal Physiol.* **283**:F447–F453.
13. Felder, R.A., and Jose, P.A. 2006. Mechanisms of disease: the role of GRK4 in the etiology of essential hypertension and salt sensitivity. *Nat. Clin. Pract. Nephrol.* **2**:637–650.
14. Crowley, S.D., et al. 2005. Distinct roles for the kidney and systemic tissues in blood pressure regulation by the renin-angiotensin system. *J. Clin. Invest.* **115**:1092–1099.
15. Ortiz, P.A., and Garvin, J.L. 2001. Intrarenal transport and vasoactive substances in hypertension. *Hypertension.* **38**:621–624.
16. Shimkets, R.A., and Lifton, R.P. 1996. Recent advances in the molecular genetics of hypertension. *Curr. Opin. Nephrol. Hypertens.* **5**:162–165.
17. Lanctôt, P.M., et al. 1999. Role of N-glycosylation in the expression and functional properties of human AT_1 receptor. *Biochemistry.* **38**:8621–8627.
18. Lanctôt, P.M., et al. 2005. Importance of N-glycosylation positioning for cell-surface expression, targeting, affinity and quality control of the human AT_1 receptor. *Biochem. J.* **390**:367–376.
19. Jose, P.A., Eisner, G.M., and Felder, R.A. 2003. Dopamine and the kidney: a role in hypertension?

Curr. Opin. Nephrol. Hypertens. **12**:189–194.

20. Wang, Q., et al. 2001. Differential dependence of the D1 and D5 dopamine receptors on the G protein 7 subunit for activation of adenylyl cyclase. *J. Biol. Chem.* **276**:39386–39393.

21. Yang, Z., et al. 2005. D5 dopamine receptor regulation of phospholipase D. *Am. J. Physiol. Heart Circ. Physiol.* **288**:H55–H61.

22. De Duve, C. 2005. The lysosome turns fifty. *Nat. Cell Biol.* **7**:847–849.

23. Goldberg, A.L. 2003. Protein degradation and protection against misfolded or damaged proteins. *Nature.* **426**:895–899.

24. Hein, L., Meinel, L., Pratt, R.E., Dzau, V.J., and Kobilka, B.K. 1997. Intracellular trafficking of angiotensin II and its AT_1 and AT_2 receptors: evidence for selective sorting of receptor and ligand. *Mol. Endocrinol.* **11**:1266–1277.

25. Dale, L.B., Seachrist, J.L., Babwah, A.V., and Ferguson, S.G. 2004. Regulation of angiotensin II type 1A receptor intracellular retention, degradation, and recycling by Rab5, Rab7, and Rab11 GTPases. *J. Biol. Chem.* **279**:13110–13118.

26. Hunyady, L., et al. 2002. Differential PI_3-kinase dependence of early and late phases of recycling of the internalized AT_1 angiotensin receptor. *J. Cell Biol.* **157**:1211–1222.

27. Finley, D., Ciechanover, A., and Varshavsky, A. 2004. Ubiquitin as a central cellular regulator. *Cell.* **116**(2 Suppl.):S29–S32.

28. Glickman, M.H., and Ciechanover, A. 2002. The ubiquitin-proteasome proteolytic pathway: destruction for the sake of construction. *Physiol. Rev.* **82**:373–428.

29. Hicke, L. 2001. A new ticket for entry into budding vesicles-ubiquitin. *Cell.* **106**:527–530.

30. Mukhopadhyay, D., and Riezman, H. 2007. Proteasome-independent functions of ubiquitin in endocytosis and signaling. *Science.* **315**:201–205.

31. Pickart, C.M., and Eddins, M.J. 2004. Ubiquitin: structures, functions, mechanisms. *Biochim. Biophys. Acta.* **1695**:55–72.

32. Wojcikiewicz, R.J. 2004. Regulated ubiquitination of proteins in GPCR-initiated signaling pathways. *Trends Pharmacol. Sci.* **25**:35–41.

33. Chen, Y., Elangovan, M., and Periasamy, A. 2005. FRET data analysis — the algorithm. In *Molecular imaging: FRET microscopy and spectroscopy.* A. Periasamy

and R.N. Day, editors. Oxford University Press. New York, New York, USA. 126–145.

34. Chen, Y., and Periasamy, A. 2004. Characterization of two-photon excitation fluorescence lifetime imaging microscopy for protein localization. *Microsc. Res. Tech.* **63**:72–80.

35. Moren, A., et al. 2005. Degradation of the tumor suppressor Smad4 by WW and HECT domain ubiquitin ligases. *J. Biol. Chem.* **280**:22115–22123.

36. Shenoy, S.K., McDonald, P.H., Kohout, T.A., and Lefkowitz, R.J. 2001. Regulation of receptor fate by ubiquitination of activated β_2-adrenergic receptor and beta-arrestin. *Science.* **294**:1307–1313.

37. Marchese, A., and Benovic, J.L. 2001. Agonist-promoted ubiquitination of the G protein-coupled receptor CXCR4 mediates lysosomal sorting. *J. Biol. Chem.* **276**:45509–45512.

38. Slagsvold, T., Brech, A., and Stenmark, H. 2006. CISK attenuates degradation of the chemokine receptor CXCR4 via the ubiquitin ligase AIP4. *EMBO J.* **25**:3738–3749.

39. Dupre, D.J., et al. 2003. Trafficking, ubiquitination, and down-regulation of the human platelet-activating factor receptor. *J. Biol. Chem.* **278**:48228–48235.

40. Jacob, C., et al. 2005. c-Cbl mediates ubiquitination, degradation, and down-regulation of human protease-activated receptor 2. *J. Biol. Chem.* **280**:16076–16087.

41. Wolfe, B.L., Marchese, A., and Trejo, J. 2007. Ubiquitination differentially regulates clathrin-dependent internalization of protease-activated receptor-1. *J. Cell Biol.* **177**:905–916.

42. Mihalik, B., et al. 2003. Endocytosis of the AT_{1A} angiotensin receptor is independent of ubiquitylation of its cytoplasmic serine/threonine-rich region. *Int. J. Biochem. Cell Biol.* **35**:992–1002.

43. Wheatley, M., and Hawtin, S.R. 1999. Glycosylation of G-protein-coupled receptors for hormones central to normal reproductive functioning: its occurrence and role. *Hum. Reprod. Update.* **5**:356–364.

44. Michineau, S., Alhenc-Gelas, F., and Rajerison, R.M. 2006. Human bradykinin B2 receptor sialylation and N-glycosylation participate with disulfide bonding in surface receptor dimerization. *Biochemistry.* **45**:2699–2707.

45. Mialet-Perez, J., Green, S.A., Miller, W.E., and Liggett, S.B. 2004. A primate-dominant third glycosylation site of the β_2-adrenergic receptor routes

receptors to degradation during agonist regulation. *J. Biol. Chem.* **279**:38603–38607.

46. Karpa, K.D., et al. 1999. N-linked glycosylation is required for plasma membrane localization of D5, but not D1, dopamine receptors in transfected mammalian cells. *Mol. Pharmacol.* **56**:1071–1078.

47. Free, R.B., et al. 2007. D1 and D2 dopamine receptor expression is regulated by direct interaction with the chaperone protein calnexin. *J. Biol. Chem.* **282**:21285–21300.

48. Jayadev, S., et al. 1999. N-linked glycosylation is required for optimal AT_{1A} angiotensin receptor expression in COS-7 cells. *Endocrinology.* **140**:2010–2017.

49. Yoshida, Y., et al. 2002. E3 ubiquitin ligase that recognizes sugar chains. *Nature.* **418**:438–442.

50. Lederkremer, G.Z., and Glickman, M.H. 2005. A window of opportunity: timing protein degradation by trimming of sugars and ubiquitins. *Trends Biochem. Sci.* **30**:297–303.

51. Crowley, S.D., et al. 2006. Angiotensin II causes hypertension and cardiac hypertrophy through its receptors in the kidney. *Proc. Natl. Acad. Sci. U. S. A.* **103**:17985–17990.

52. Cheng, H.F., Becker, B.N., and Harris, R.C. 1996. Dopamine decreases expression of type-1 angiotensin II receptors in renal proximal tubule. *J. Clin. Invest.* **97**:2745–2752.

53. Salomone, L.J., et al. 2007. Intrarenal dopamine D1-like receptor stimulation induces natriuresis via an angiotensin type-2 receptor mechanism. *Hypertension.* **49**:155–161.

54. Caron, K.M., et al. 2002. A genetically clamped renin transgene for the induction of hypertension. *Proc. Natl. Acad. Sci. U. S. A.* **99**:8248–8252.

55. Matchar, D.B., et al. 2008. Systematic review: comparative effectiveness of angiotensin-converting enzyme inhibitors and angiotensin II receptor blockers for treating essential hypertension. *Ann. Intern. Med.* **148**:16–29.

56. Ladasky, J.J., et al. 2006. Bap31 enhances the endoplasmic reticulum export and quality control of human class I MHC molecules. *J. Immunol.* **177**:6172–6181.

57. Lakowicz, J.R., Piszczek, G., and Kang, J.S. 2001. On the possibility of long-wavelength long-lifetime high-quantum-yield luminophores. *Anal. Biochem.* **288**:62–75.